Crystal-Face Dependence and Photoetching-Induced Increases of Dye-Sensitized Photocurrents at Single-Crystal Rutile TiO_2 Surfaces

Akihito Imanishi,[†,§] Hidenori Suzuki,[†] Kei Murakoshi,[‡] and Yoshihiro Nakato*[,†,§]

Division of Chemistry, Graduate School of Engineering Science, Osaka University, Toyonaka, Osaka 560-8531, Japan, Department of Chemistry, Graduate School of Science, Hokkaido University, Sapporo, Hokkaido 060-0810, Japan, and Core Research for Evolutional Science and Technology (CREST), JST, 4-1-8, Honmachi, Kawaguchi, Saitama 332−0012, Japan

Received: December 28, 2005; In Final Form: June 15, 2006

Dye-sensitized photocurrents at (100)-, (001)-, and (110)-cut TiO_2 rutile surfaces were increased by photoetching of TiO_2, but the increasing ratio strongly depended on the cut crystal faces and the illumination intensity for the photoetching. For the (110)-cut surface, the photocurrent increase was moderately large and in proportion to the increase in the surface area of TiO_2 induced by the photoetching, irrespective of the illumination intensity for the photoetching. On the other hand, the photocurrent increases for the (001)- and (100)-cut surfaces, especially that for the (001)-cut surface, were prominent and largely exceeded the increases in the surface area. The results were explained by taking into account the following factors: (1) The (001)- and (100)-cut surfaces were thermodynamically unstable in contrast to the (110)-cut surface and had thicker inactive surface layers (or higher densities of surface defects), produced by surface reconstruction during heat treatment of TiO_2 at 550 °C in a hydrogen atmosphere for getting n-type semiconductivity. (2) Photoetching not only increased the surface area through formation of nanoholes and grooves at the surface but also effectively removed the thin inactive surface layers (or surface defects).

Introduction

Dye-sensitized photoelectrochemical solar cells (DSSC)[1−4] have attracted much interest in view the of possibilities of high energy conversion efficiency and low production cost.[5−8] They have made steady progress in both efficiency and stability in this decade. For nanocrystalline TiO_2 photoelectrodes,[9−11] morphological properties of the electrode and electronic structures at the TiO_2 surface play important roles in the increase in efficiency. For example, the particle size and the size of pores between particles will determine the extent of grain boundaries, the real surface area of the electrode in contact with the electrolyte, and the rate of charge transfer and diffusion of active species in the electrode. On the other hand, surface defects or surface states at the TiO_2 surface will induce effective back electron transfer from the electrode to the electrolyte, finally exerting a strong influence on the photovoltaic properties of the photoelectrode.

The effective production of ordered well-defined nanostructures is, in general, the central issue of modern device technologies. Development of new techniques for producing such structures is strongly desired to fabricate high-performance optical and electronic nanodevices.[12−14] The control size of a few to several tens of nanometers is in general beyond the control size of the conventional photolithographic technique, which is in the range of >100 nm. Atomic-scale fabrication by means of scanning probe microscopy[15] has, unfortunately, a severe limit in that it is not adaptable to mass production eventually necessary for practical application.

The chemical and electrochemical methods to produce nanostructures by making use of self-organizing abilities of molecular systems are promising approaches to the solution of the above problem. Some examples of spontaneous ordering of metal[16] and semiconductor[17,18] nanoparticles and formation of domain structures in self-assembled monolayers[19] were reported. We have also been studying the formation of nanosized ordered structures, such as aligned nanoholes[20] and nanorods,[21−23] ordered arrays of nanodots,[24,25] and ordered step structures[26,27] on single-crystal semiconductor and metal surfaces, with the aim of exploring new effective techniques for the production of ordered nanostructures.

Recently, we found that photoetching of single-crystal n-TiO_2 (rutile) surfaces in an aqueous sulfuric acid solution produced fairly well arranged nanometer-sized rectangular holes and grooves, extending in the ⟨001⟩ direction and having selectively the (100) face at the walls.[28,29] Interestingly, the (100) surface exposed by the photoetching was nearly atomically flat, as indicated by an appearance of a photoluminescence (PL) band peak at 840 nm,[28,29] which completely disappeared for atomically roughened TiO_2 surfaces.[30] Although many studies have been reported on the formation of porous structures on solid surfaces (e.g., porous Al_2O_3[31,32] and porous Si[33]), there are few examples for nanostructures with well-defined crystal surfaces such as photoetched TiO_2 surfaces.

In this work, we have studied crystal-face dependences of the dye-sensitized photocurrents at n-TiO_2 rutile surfaces, using (100)-, (001)-, and (110)-cut and photoetched [the (100)-face exposed] surfaces. For nanocrystalline TiO_2 photoelectrodes normally used for dye sensitization,[9−11] each TiO_2 particle will expose various crystal faces at the surface. Therefore, it is of high importance to investigate crystal-face dependences of the dye-sensitized photocurrents and clarify ill-behaving surfaces in the TiO_2 particle, for improving the electrode performance.

* To whom correspondence should be addressed. Fax: +81-6-6850-6236. E-mail: nakato@chem.es.osaka-u.ac.jp.
† Osaka University.
‡ Hokkaido University.
§ JST.

10.1021/jp057538h CCC: $33.50 © 2006 American Chemical Society
Published on Web 09/23/2006

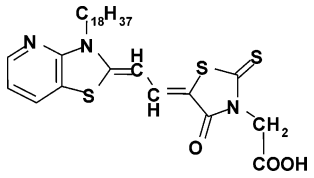

Figure 1. Structure of benzothiazole merocyanine dye, abbreviated as Mc[18,1].

Experimental Section

Single-crystal TiO_2 (rutile) wafers of 99.99% purity, 10 × 10 mm area, and 1.0 mm thick, having (001)-, (100)-, and (110)-cut and alkali-polished[34] surfaces, were obtained from Earth Chemical Co. The wafers were simply washed with pure water and reduced in a stream of hydrogen at 550 °C for 30 min to get n-type semiconductivity.[28,29] The electrodes were prepared by making ohmic contact on TiO_2 surfaces with indium−gallium alloy and mounting them in a Teflon holder (effective area 0.25 cm^2).

Photoetching was carried out in 0.05 M H_2SO_4 using a three-electrode photoelectrochemical cell with a Pt plate as the counter electrode and an Ag/AgCl/KCl(satd) electrode as the reference electrode. The electrode potential was kept at +2.5 V during UV illumination with a 500-W super high pressure mercury lamp as the light source. The illumination was carried out from the side of the TiO_2 surface. The electrolyte solution was stirred magnetically and kept at 20 ± 0.3 °C during the illumination. The nanostructure of the TiO_2 surface was inspected with a high-resolution scanning electron microscope (Hitachi, S-5000) and an atomic force microscope (Digital Instruments, Nanoscope IIIa).

Dye-sensitized photocurrent density (*j*) versus potential (*U*) curves were measured by illumination with a 300-W Xe lamp combined with a monochromator, using a commercial potentiostat and a potential programmer. Benzothiazole merocyanine (abbreviated as Mc[18,1]), whose structure is shown in Figure 1, was used as the dye. Sayama et al. reported that the long alkyl chain led to formation of fine packing of the dye chromophores important for a high incident photon to current conversion efficiency (IPCE).[35] Before dye adsorption, as-cut or photoetched TiO_2 was pretreated at 100 °C in air for 12 h, and then immersed in an aqueous EtOH solution of Mc[18,1] for 18 h. The Pt plate (2 × 3 cm^2) and the Ag/AgCl/saturated KCl electrode were used as the counter electrode and the reference electrode, respectively. The electrolyte for all the measurements was acetonitrile with 0.15 M LiI. It was prepared by use of reagent grade chemicals. The concentration unit mol/dm^3 is abbreviated as "M" in the present paper. The amount of adsorbed dye molecules was investigated by measurements of the S 2p X-ray photoelectron spectroscopic (XPS) peak. The binding energy and the intensity for the XPS peak were calibrated by using the Ti $2p_{1/2}$ peak at 458.7 eV from TiO_2 crystal as the reference. XPS spectra were obtained with a Shimadzu ESCA 1000 spectrometer, with an Al Kα line (1486.6 eV) as the X-ray source.

Results

Figure 2 shows scanning electron microscopic (SEM) images for the (110)-, (100)-, and (001)-cut TiO_2 single-crystal surfaces (Figure 2a) before and (Figure 2b−d) after photoetching, where the intensity of illumination for the photoetching is changed from (b) 10 to (c) 20 and (d) 40 mW/cm^2. The electricity passing across the electrode surface during the photoetching was in all cases kept at 50 C/cm^2 for the apparent area of the electrode surface.

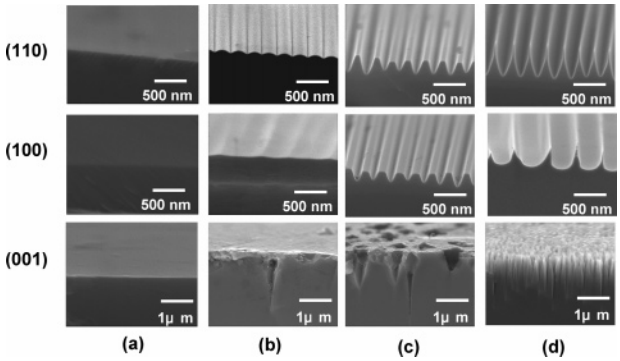

Figure 2. SEM images for (110)-, (100)-, and (001)-cut TiO_2 single-crystal surfaces (a) before and (b−d) after photoetching with UV illumination, where the intensity of illumination is changed from (b) 10 to (c) 20 and (d) 40 mW/cm^2. The electricity passing across the electrode surface during the photoetching was 50 C/cm^2 for the apparent area of all electrode surfaces.

We can see that the morphology of the TiO_2 surface after photoetching strongly depends on the cut crystal surfaces and the illumination intensity for the photoetching. Photoetching of the (001)-cut surface with 10 mW/cm^2 illumination gave sparsely distributed rectangular holes (or pits) with an inverse-pyramid shape. On the other hand, regularly arranged shallow grooves were formed at the (110)- and (100)-cut surfaces. The holes or grooves grew with the increasing intensity of UV illumination, accompanied by increases in the TiO_2 surface area. We should note that the photoproduced nanoholes or grooves extended in the ⟨001⟩ direction and had selectively the (100) face at the walls, irrespective of the cut crystal faces of the electrodes.[28] The extension of the nanoholes and grooves in the ⟨001⟩ direction can be explained by the presence of crystalline channels for rutile-type TiO_2 in this direction, which will lead to a high photoetching rate along this direction. The selective exposition of the (100) face at the photoetched surfaces was explained by considering a kinetics-controlled mechanism, the details of which were described in a previous paper.[29]

Figure 3 shows incident photon to current conversion efficiency (IPCE) spectra (Figure 3a) and XPS S 2p spectra (Figure 3b) for the (110)-, (100)-, and (001)-cut TiO_2 surfaces before photoetching. The IPCE value strongly depended on the cut faces and was in the order (110)-cut > (100)-cut > (001)-cut surfaces. In particular, the IPCE value for the (110)-cut surface was very high compared with those for the other two surfaces. On the other hand, the amount of adsorbed dye molecules estimated from the intensity of the XPS S 2p peak was in the order (001)-cut > (100)-cut > (110)-cut surfaces, which is the inverse of the order of the IPCE value. The XPS S 2p peak showed no satellite (or shoulder) band attributable to, e.g., atomic S, suggesting no decomposition of the dye at the TiO_2 surface. In addition, mutual differences in the amount of adsorbed dye are much smaller than those in the IPCE value. These results indicate that the high IPCE value for the (110)-cut surface is not attributable to a difference in the amount of adsorbed dye molecules.

Figure 4 shows the IPCE spectra for the (110)-, (100)-, and (001)-cut TiO_2 surfaces after photoetching with 10 (Figure 4a), 20 (Figure 4b), and 40 (Figure 4c) mW/cm^2 illumination. By the photoetching with the 10 mW/cm^2 illumination, the IPCE values for all the cut surfaces increased from those for the

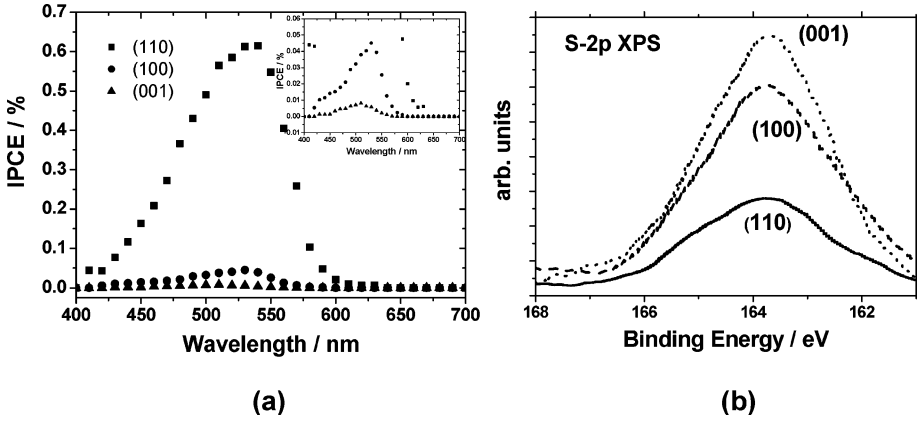

Figure 3. IPCE (a) and S 2p XPS (b) spectra for (110)-, (100)-, and (001)-cut TiO_2 surfaces before photoetching. The inset in (a) displays the IPCE spectra on an expanded scale in the IPCE axis.

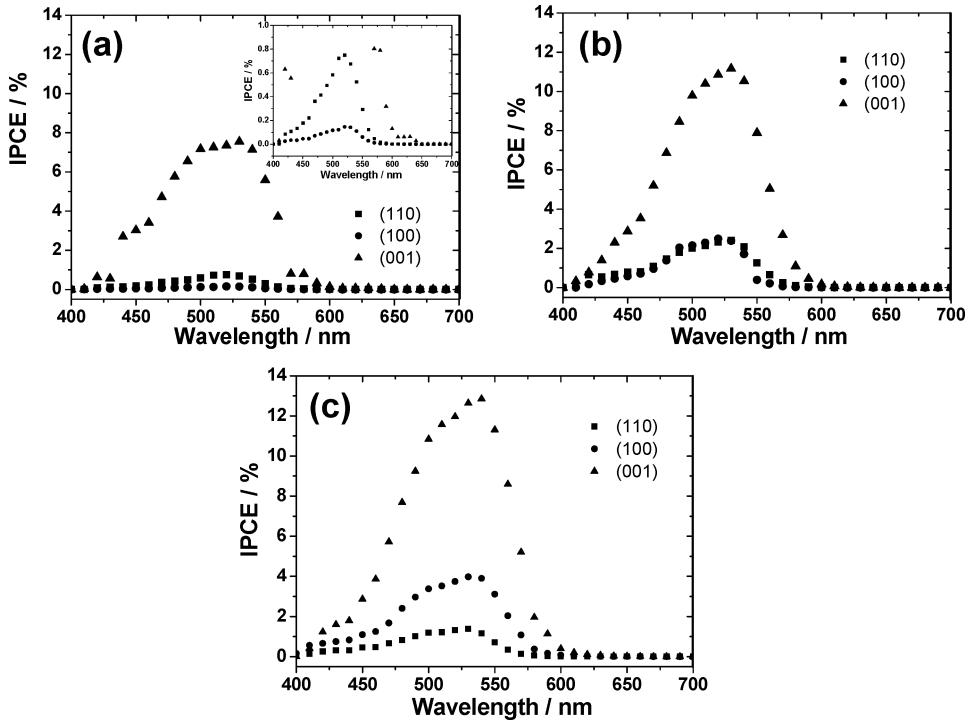

Figure 4. IPCE spectra for (110)-, (100)-, and (001)-cut TiO_2 single-crystal surfaces after photoetching with 10 (a), 20 (b), and 40 (c) mW/cm^2 illumination. The inset displays the IPCE spectra on an expanded scale in the IPCE axis.

nonphotoetched surfaces. Especially the IPCE value for the (001)-cut surface, which was the smallest before the photoetching, was remarkably enhanced, thus leading to a change in the order of the IPCE value such as the (001)-cut > (110)-cut > (100)-cut surfaces. The IPCE values for all the cut surfaces increased further by the 20 and 40 mW/cm^2 illumination, but the order of the IPCE values did not change in these cases.

To investigate reasons why such remarkable crystal-face dependences appeared for the IPCE enhancement by the photoetching, we tried to measure directly the amount of adsorbed dye molecules on the photoetched TiO_2 surfaces either by measurements of absorption spectra of solutions into which adsorbed dye molecules are dissolved or by measurements of XPS spectra. Unfortunately, we failed to get reliable data from both methods. The amount of adsorbed dye was too small to be measured by the absorption spectra. On the other hand, for the XPS experiment, both the S 2p and Ti 2p peak intensities were largely scattered from experiment to experiment, probably owing to the nonflat character of the photoetched TiO_2 surfaces. It may be pointed out here that relatively low IPCE values in Figure 4 are only due to small surface areas of single-crystal electrodes (or weak light absorption of adsorbed dye molecules). In fact, a quite rough estimation of the absorbed photon to current conversion efficiency (APCE) for the (100)-cut surface after the 10 mW/cm^2 photoetching suggested that it was nearly comparable to the value reported by the other group.[35]

Discussion

Let us first consider the dye-sensitized photocurrents at the nonphotoetched (as-cut, apparently flat) TiO_2 surfaces (Figures 2a and 3). The IPCE value for the (110)-cut surface is very high compared with those for the other two surfaces. The difference in the IPCE values cannot be attributed to the difference in the amount of adsorbed dye molecules, as already mentioned in the preceding section. Another plausible factor affecting the

IPCE value is a difference in the surface (electronic) structure of the TiO_2 electrode.

It is known[36] that the (110) surface is the thermodynamically most stable among the various TiO_2 surfaces. In fact, the (110) surface is not reconstructed even by annealing at a high temperature of 1150 K, whereas the (100) and (001) surfaces are easily reconstructed by annealing at much lower temperatures.[36−39] We reported previously that heat treatments of single-crystal TiO_2 wafers at 700 °C[28] and even at 550 °C[29] in a hydrogen atmosphere for getting n-type semiconductivity produced thin inactive (distorted or amorphous) surface layers (or surface defects) exerting a severe detrimental effect on (water oxidation) photocurrent density vs potential curves. The layers (or the detrimental effect) were removed easily by photoetching, i.e., by first several cyclic potential scans under illumination in 0.05 M H_2SO_4.[28,29] The surface damage caused by the heat treatments was most serious for the (001)-cut surface and much less for the (110)-cut surface,[28,29] suggesting that it is due to surface reconstruction under the heat treatments. The TiO_2 electrodes in the present work were also heat treated at 550 °C under H_2 and are expected to have damaged surface layers, especially for the thermodynamically unstable (001)- and (100)-cut surfaces. This can explain well why the (110)-cut surface gave the highest photocurrent with the smallest adsorbed dye molecules, before the photoetching. This argument is also supported by large increases in the IPCE for the (001)- and (100)-cut surfaces by photoetching, as discussed below.

After photoetching with the 10 mW/cm^2 illumination, the IPCE value of the (001)-cut surface was strongly enhanced, whereas that of the (110)-cut surface was just weakly increased. Why did the IPCE increase by photoetching strongly depend on the kind of the cut surfaces? For photoetching with the 10 mW/cm^2 illumination, the formation of the nanoholes or grooves does not proceed much, with only shallow grooves or sparsely distributed holes being formed at the surface (Figure 2b). This implies that there is not a large difference in surface area among the (110)-, (100)-, and (001)-cut surfaces after photoetching. It should be noted also that, after photoetching, only the (100) face is exposed at all cut surfaces and thus the adsorption behavior of dye molecules is nearly the same among the (110)-, (100)- and (001)-cut surfaces. In addition, our previous work[28,30] shows that the (100) surface exposed by photoetching is atomically nearly flat and has no nanometer-scale roughness, as mentioned in the Introduction. These facts indicate that the amount and structure of adsorbed dye molecules are nearly the same among the (110)-, (100)-, and (001)-cut surfaces after the 10 mW/cm^2 photoetching and thus cannot explain the aforementioned large difference in the photoetching-induced IPCE enhancement among these cut surfaces.

Here we should note that we mentioned earlier that the (001)- and (100)-cut surfaces before photoetching had thin inactive (distorted or amorphous) surface layers (or surface defects) exerting a severe detrimental effect on (water oxidation) photocurrent density vs potential curves. Thus, if the photoetching removes such inactive layers (or surface defects), this should induce drastic increases in the photocurrent, as observed in experiments. On the other hand, the (110) surface is thermodynamically stable and not reconstructed under the heat treatment, and thus the (110)-cut surface before photoetching had little inactive surface layer (or surface defects). In such a case, the photocurrent was hardly increased by the photoetching, also in agreement with the experiment.

For the photoetching with 20 and 40 mW/cm^2 illumination, the deep grooves or dense holes are formed at the surfaces (Figure 2c,d), accompanied by large increases in the surface area of the TiO_2 electrodes. The IPCE values in these cases are equally enhanced for all the cut surfaces, in harmony with the increases in the surface area of the electrodes. The large difference in the IPCE enhancement among the three cut surfaces, such as observed for the photoetching with the 10 mW/cm^2 illumination, was not observed in these cases.

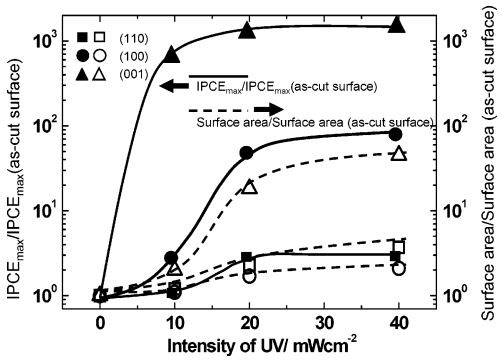

Figure 5. Plots of surface area (broken curves) and maximum IPCE value (solid curves) against intensity of UV illumination for photoetching. Both the surface area and the IPCE are normalized for the corresponding values for the as-cut surface. The circular, triangular, and square symbols represent the data for the (100)-, (001)-, and (110)-cut surfaces, respectively.

Let us now consider again the two important factors of the photoetching: (1) the removal of inactive surface layers (or decrease in the densities of surface defects) and (2) the increase in the surface area. Figure 5 plots the maximum IPCE value ($IPCE_{max}$) as well as the surface area of the electrode against the intensity of the UV illumination for the photoetching. Both the IPCE and the surface area are normalized for the corresponding values for the as-cut surfaces (i.e., the surfaces before photoetching). The surface area was estimated from the geometries of the TiO_2 surfaces in the SEM images. For example, for the (001) surfaces photoetched with 20 and 40 mW/cm^2 illumination, the surface areas were calculated by assuming that the nanoholes had shapes of quadrangular pyramid and quadrangular prism, respectively, with the length, the width, and the density of the nanoholes being estimated from the SEM images. As mentioned earlier, only the (100) face was selectively exposed at the photoetched surfaces, irrespective of the kind of cut surfaces. Moreover, the photoetched surface is atomically nearly flat and has no nanometer-scale roughness. Accordingly, we can expect that the surface area for the photoetched surface in Figure 5 is nearly in proportion to the amount of the adsorbed dye.

For the (110)-cut surface, the increase in the $IPCE_{max}$ with the illumination intensity nearly agrees with the increase in the surface area, indicating that the increase in the IPCE for this surface is mainly due to the increase in the surface area (or in the amount of the adsorbed dye). On the other hand, for the (100)- and (001)-cut surfaces, the increases in the $IPCE_{max}$ with the illumination intensity are significantly larger than the increases in the surface area, suggesting that the increases in the IPCE for these surfaces are induced not only by the increase in the surface area but also by the removal of the inactive surface layers (or surface defects). The difference between the (110)-cut and (100)- or (001)-cut surfaces can be explained by taking into account the difference in the thermodynamic stabilities of the crystal faces, as mentioned earlier.

Another notable point in Figure 5 is that the increase in the IPCE for the (001)-cut surface by photoetching with 10 mW/cm^2 illumination is quite prominent. This suggests that the

inactive surface layers (or surface defects) at the (001)-cut surface were removed enough by the photoetching at a low illumination intensity. Almost no increase in the IPCE for the (001)-cut surface by photoetching at the high-intensity illumination (Figure 5), despite the increase in the surface area through the formation of dense long nanoholes (Figure 2), might be attributed to slow diffusion of dye molecules with the long alkyl chain (Figure 1) into the long nanoholes, resulting in little dye adsorption inside the nanoholes.

In relation to the above argument, we should note also that the (001)-cut surface even after the photoetching at the low illumination intensity yielded the highest photocurrent among the three cut surfaces (Figure 4). This prominent feature for the (001)-cut surface may partly arise from the dependence of the mobility of photogenerated holes and electrons on the crystal direction. Considering the presence of crystalline channels for rutile-type TiO_2 in the ⟨001⟩ direction, the holes and electrons may diffuse much faster in this direction,[28] resulting in a high photocurrent for the photoetched (001)-cut surface.

We have mentioned earlier that we can expect that the surface area for the photoetched surface in Figure 5 to be nearly in proportion to the amount of the adsorbed dye. One might point out, however, that this expectation does not hold between the nonphotoetched and photoetched surfaces because they have different crystal faces and thus differing adsorption behavior of the dye. This problem has remained unresolved because we failed to get reliable data in the measurements of the amount of the adsorbed dye for the photoetched surfaces, as mentioned in the preceding section. It should be noted here that the difference in the amount of the adsorbed dye among various crystal faces is estimated, from Figure 3b, to be within several times, whereas the IPCE enhancement by the photoetching reaches several tens to several hundreds of times (Figure 5). Thus, we can safely say that the aforementioned discussion and conclusions are essentially valid, apart from detailed arguments on small differences.

Conclusion

The crystal-face dependence and the photoetching-induced enhancement of the dye-sensitized photocurrents at the TiO_2 rutile surfaces were investigated, using (100)-, (001)-, and (110)-cut and photoetched TiO_2 surfaces. The photocurrents at all cut surfaces were increased by the photoetching, but the increasing ratio strongly depended on the cut surfaces. The results were explained by considering two factors of the photoetching: (1) the removal of the inactive surface layers (or surface defects) at the TiO_2 surface, produced by surface reconstruction during the heat treatment, and (2) the increase in the surface area through the formation of nanosized holes and grooves. In particular, the (001)- and (100)-cut surfaces showed much larger increases in the photocurrent than the increase in the surface area, clearly indicating the importance of the removal of the inactive surface layers (or surface defects) at thermodynamically unstable crystal surfaces. It was also discussed that the dependence of the mobility of photogenerated electrons and holes on the crystal direction plays a role in the magnitude of the photocurrent.

Acknowledgment. This work was partially supported by a program of NEDO (Project ID 02B69006c), Japan.

References and Notes

(1) Gerischer, H.; Michel-Beyerle, M. E.; Rebentrost, F.; Tributsch, H. *Electrochim. Acta* **1968**, *13*, 1509−1515.
(2) Gerischer, H.; Tributsch, H. *Ber. Bunsen-Ges. Phys. Chem.* **1968**, *72*, 437−445.
(3) Tsubomura, H.; Matsumura, M.; Nomura, Y.; Amamiya, T. *Nature* **1976**, *261*, 402−403.
(4) Watanabe, T.; Fujishima, A.; Tatsuoki, O.; Honda, K. *Bull. Chem. Soc. Jpn.* **1976**, *49*, 8−11.
(5) O'Regan, B.; Gratzel, M. *Nature* **1991**, *353*, 737−740.
(6) Nazeeruddin, M. K.; Kay, A.; Rodicio, I.; Humphry-Baker, R.; Muller, E.; Liska, P.; Vlachopoulos, N.; Gratzel, M. *J. Am. Chem. Soc.* **1993**, *115*, 6382−6390.
(7) Hagfeldt, A.; Gratzel, M. *Chem. Rev.* **1995**, *95*, 49−68.
(8) Burnside, S. D.; Brooks, K.; McEvoy, A. J.; Gratzel, M. *Chimia* **1998**, *52*, 557.
(9) Gomez, M. M.; Lu, J.; Olsson, E.; Hagfeldt, A.; Granqvist, C. G. *Sol. Energy Mater. Sol. Cells* **2000**, *64*, 385−392.
(10) Huang, S. Y.; Schlichthörl, G.; Nozik, A. J.; Grätzel, M.; Frank, A. J. *J. Phys. Chem. B* **1997**, *101*, 2576−2582.
(11) Pichot, F.; Gregg, B. A. *J. Phys. Chem. B* **2000**, *104*, 6−10.
(12) Ashoori, R. C. *Nature* **1996**, *379*, 413−419.
(13) Kiely, C. J.; Fink, J.; Brust, M.; Bethell, D.; Schiffrin, D. J. *Nature* **1998**, *396*, 444−446.
(14) Timp, G. *Nanotechnology*; Springer-Verlag: New York, 1999.
(15) Nyffenegger, R. M.; Penner, R. M. *Chem. Rev.* **1997**, *97*, 1195−1230.
(16) Pileni, M. M. *New J. Chem.* **1998**, 693.
(17) Fendler, J. H. *Chem. Mater.* **1996**, *8*, 1616−1624.
(18) Murray, C. B.; Kagan, C. R.; Bawendi, M. G. *Science* **1995**, *270*, 1335−1338.
(19) Ulman, A. *Chem. Rev.* **1996**, *96*, 1533−1554.
(20) Morisawa, K.; Ishida, M.; Yae, S.; Nakato, Y. *Electrochim. Acta* **1999**, *44*, 3725−3729.
(21) Imanishi, A.; Ishida, M.; Zhou, X.; Nakato, Y. *Jpn. J. Appl. Phys.* **2000**, *39*, 4355−4358.
(22) Imanishi, A.; Morisawa, K.; Nakato, Y. *Electrochem. Solid-State Lett.* **2001**, *4*, C69−C72.
(23) Imanishi, A.; Hayashi, T.; Nakato, Y. *Langmuir* **2004**, *20*, 4604−4608.
(24) Murakoshi, K.; Nakato, Y. *Jpn. J. Appl. Phys., Part 1* **2000**, *39* (7B), 4633−4634.
(25) Murakoshi, K.; Nakato, Y. *Adv. Mater.* **2000**, *12*, 791−795.
(26) Imanishi, A.; Nagai, T.; Nakato, Y. *J. Phys. Chem. B* **2004**, *108*, 21−23.
(27) Nagai, T.; Imanishi, A.; Nakato, Y. *Appl. Surf. Sci.* **2004**, *237*, 532−536.
(28) Tsujiko, A.; Kisumi, T.; Magari, Y.; Murakoshi, K.; Nakato, Y. *J. Phys. Chem. B* **2000**, *104*, 4873−4879.
(29) Kisumi, T.; Tsujiko, A.; Murakoshi, K.; Nakato, Y. *J. Electroanal. Chem.* **2003**, *545*, 99−107.
(30) Nakamura, R.; Okamura, T.; Ohashi, N.; Imanishi, A.; Nakato, Y. *J. Am. Chem. Soc.* **2005**, *127*, 12975−12983.
(31) Keller, F.; Hunter, M.; Robinson, D. L. *J. Electrochem. Soc.* **1953**, *100*, 411.
(32) Huber, C. A.; Huber, T. E.; Sadoqi, M.; Lubin, J. A.; Manalis, S.; Prater, C. B. *Science* **1994**, *263*, 800−801.
(33) Canham, L. T. *Appl. Phys. Lett.* **1990**, *57*, 1046−1048.
(34) The details of the alkali polishing adopted by the company are unknown, being kept secret.
(35) Sayama, K.; Tsukagoshi, S.; Hara, K.; Ohga, Y.; Shinpou A.; Abe, Y.; Suga, S.; Arakawa, H. *J. Phys. Chem. B* **2002**, *106*, 1363−1371.
(36) Tero, R.; Fukui, K.; Iwasawa, Y. *J. Phys. Chem. B* **2003**, *107*, 3207−3214.
(37) Onishi, H.; Iwasawa, Y. *Surf. Sci.* **1994**, *313*, L783−L789.
(38) Hardman, P. J.; Prakash, N. S.; Muryn, C. A.; Raikar, G. N.; Thomas, A. G.; Prime, A. F.; Thornton, G.; Blake, R. *Phys. Rev. B* **1993**, *47*, 16056−16059.
(39) Diebold, U. *Surf. Sci. Rep.* **2003**, *48*, 53−229.